PHYSICAL REVIEW B VOLUME 47, NUMBER 17 1 MAY 1993-I

Efficient calculation of high-order self-energy corrections to phonon linewidths: Application to α-nitrogen

Piero Procacci and Giorgio Federico Signorini
Dipartimento di Chimica, Universitá di Firenze, via Gino Capponi 9, I-50121, Firenze, Italy

Raffaele Guido Della Valle
Dipartimento di Chimica-Fisica e Inorganica, Universitá di Bologna, Viale Risorgimento 4, I-40136 Bologna, Italy
(Received 19 November 1992)

This paper presents an efficient method for computing high-order corrections to phonon linewidths in crystals. Traditional algorithms involve nested sums over intermediate phonon states, whose computational time grows exponentially with the perturbation order. This nested-sum difficulty is overcome in the present study for the special case of the double-vertex diagrams by writing the corresponding linewidths in a simple form and exploiting a recursive algorithm for weighted phonon densities of states, which requires a time linear in the perturbation order. Using this method, we computed, up to order 10, the linewidths due to the double-vertex diagrams for the α-nitrogen crystal. Our calculation shows that accurate estimates of high-order linewidth corrections can be obtained even for systems as complex as molecular crystals.

I. INTRODUCTION

Homogeneous line broadening in crystals is due to the anharmonicity of the interaction potential. In harmonic solids, the dynamics is described by a set of independent oscillators, the normal modes of vibration. In second quantization these vibrational excitations are described in terms of noninteracting bosons (phonons). In anharmonic solids, phonons are no longer independent, i.e., they can exchange energy. The energy transfer among phonons is responsible for the finite lifetime of vibrational excitations, and thus for the occurrence of line broadening.

Experimental linewidths for a number of molecular crystals have been measured by coherent anti-Stokes Raman spectroscopy (CARS) and high-resolution Raman techniques (for a review of the experimental studies see Refs. 1 and 2). The interpretation of the observed linewidths in terms of decay mechanisms is generally based on the temperature dependence of the linewidths.

Theoretical linewidths can be computed by perturbation expansion of the one-phonon Green's function.[3–7] The high-temperature linewidths are directly proportional to the temperature if the Green's function is restricted to the lowest order (λ^2 order) in the Van Hove perturbation parameter λ.[4,8] Nonlinear temperature dependences imply decay mechanisms at least of order λ^4. It is generally believed that mechanisms of order higher than λ^2 play a major role in the broadening of phonon lines,[9–12] since nonlinear temperature dependences have been often observed in a variety of solids.[1,2] However, a clear understanding of the high-order phonon interactions is still lacking.

So far, calculations on real systems have been done at the lowest perturbation order (λ^2).[13–19] Calculations including higher-order terms are still at a pioneeristic level, due to the huge computational cost. The λ^4 corrections have been computed either using drastic approximations[10] or simple models such as linear chains of atoms[11] or molecules.[12] In all cases they have been found to yield the largest contribution to the linewidths even at relatively low temperature. It is, however, still a matter of discussion whether for real systems convergence of the self-energy is reached at the order λ^4 in the whole temperature range of existence of solids. Rough estimates of the high-order self-energy have been suggested for linear chains,[9,12] but no attempt has been made so far to extend the perturbative approach beyond λ^4 for molecular solids.

In this paper we address the problem of computing accurate estimates of some high-order corrections to the linewidths in real molecular crystals. The large computational cost of high-order corrections is due to the fact that they involve multiple wave-vector sums. These sums must be evaluated by sampling a number N of wave vectors in the Brillouin zone. The computing time for n-nested sums grows *exponentially* as N^n, quickly exceeding any reasonable limit.

This problem is partially overcome in this paper by exploiting previous works.[20,21] The main results of Ref. 20 is a very efficient recursive algorithm for computing the multiphonon density of states, which requires a *linear* time proportional to Nn. The algorithm is applicable to weighted densities of states with a "factorized"[20] weight function. Reference 21 is based on a new interpretation of the phonon operators. In this picture the annihilation of a phonon with energy ω (and wave vector $\mathbf{k}$) is described as the creation of an "antiphonon" with negative energy $-\omega$ (and wave vector $-\mathbf{k}$). Such a description yields extremely compact expressions for the anharmonic corrections to the self-energy.

The perturbation expansion of the Green's function is best expressed as a sum on diagrams. In this work we

have selected a physically important subset of diagrams, the double-vertex diagrams (Fig. 1). The double-vertex diagrams seem to dominate the decay of high-energy vibrons.[18,22] Moreover, diagrams of this kind often appear as self-energy insertions in more complicated irreducible diagrams. The behavior of the double-vertex diagrams is therefore of paramount importance for the understanding of the overall convergence properties of the complete self-energy series. In the phonon-antiphonon picture, the linewidth due to these diagrams has a particularly simple representation involving weighted density of states generalized to allow both positive and negative phonon energies.[21] The weight functions are a combination of thermal factors and potential derivatives and, unfortunately, are not factorizable, so that the recursive algorithm cannot be used. We have succeeded in expressing the thermal factor in terms of factorized functions and chosen an approximation in which the potential derivatives are factorized.

Recently, the linewidths of the vibron in the α phase of nitrogen have been measured with great accuracy as a function of temperature by means of high-resolution Raman[23,24] and CARS techniques.[25] The linewidths of the Raman-active lattice modes are also available at several temperatures.[23,27] Therefore, we have chosen nitrogen as a benchmark for our method. The linewidths up to the order λ^{10} have been computed.

The paper is organized as follows. In Sec. II we derive a general expession for the double-vertex diagram of order n and describe how the thermal factors are factorized. In Sec. III we describe the calculations of the high-order contributions to phonon linewidths in nitrogen. First, we outline a simple numerical method for estimating the anharmonic coupling coefficients, and discuss how the thermally weighted densities may be efficiently computed. Then, the phonon linewidths are obtained by multiplying the average scattering coefficients by the thermally weighted density of states. The temperature behavior of the computed linewidths for all the Raman modes (the internal vibrons and the lattice phonons) is compared to the experimental data[23–27] in Sec. IV. Comparison to experiment is discussed in terms of decay processes.

II. THEORY

The spectrum of a phonon system is described by the one-phonon Green's function $G(b_{\mathbf{k}i}, b^{\dagger}_{\mathbf{k}i};\omega)$.[3–7] The operator $b_{\mathbf{k}i}$ and its adjoint $b^{\dagger}_{\mathbf{k}i}$ annihilate and create phonons with wave vector $\mathbf{k}$ and unperturbed (harmonic) energy ω_{ki}. The index i distinguishes different phonon branches with the same wave vector. When no ambiguity is possible, we will replace each pair of indices $\mathbf{k}i$ with a single label: $q \equiv \mathbf{k}_q i_q$ and $-q \equiv -\mathbf{k}_q - i_q$. In this work we adopt the formalism of Ref. 21, and allow both positive and negative signs of the branch indices. The positive or negative sign distinguishes between annihilation and creation operators $b_{\mathbf{k}i}$ and $b^{\dagger}_{\mathbf{k}i}$:

$$b_{\mathbf{k}i} \equiv b^{\dagger}_{-\mathbf{k}-i} \quad \text{for } i<0 \ . \tag{2.1}$$

The phonon energy is positive or negative according to the sign $\sigma_i \equiv \text{sign}(i)$ of the branch index:

$$\omega_{\mathbf{k}i} \equiv \sigma_i |\omega_{\mathbf{k}i}| \ . \tag{2.2}$$

For anharmonic solids the Green's function for the $q \equiv \mathbf{k}_q i_q$ phonon has the form[8]

$$G(b_q, b_{-q};\omega) = \frac{1}{\omega - \omega_q - \Sigma_q} \ , \tag{2.3}$$

where $\Sigma_q = \Delta_q + i\Gamma_q$ is the phonon self-energy given by the sum of all irreducible diagrams. The real part Δ_q represents an energy shift whereas the imaginary part Γ_q is the inverse of the phonon decay time, and represents an energy damping. The phonon linewidth is twice the damping Γ_q.

As shown in Ref. 21, the Green's function may be computed using the equation of motion formalism.[5,6] An infinite chain of coupled equations is obtained with an iterative procedure. In this work we truncate the chain after the first two iterations and restrict our attention to phonon-scattering processes represented by double-vertex diagrams. A double-vertex diagram is made of two vertices of order n connected by $n-1$ phonon lines. Double-vertex diagrams of this kind are shown in Fig. 1 up to the order λ^{10}.

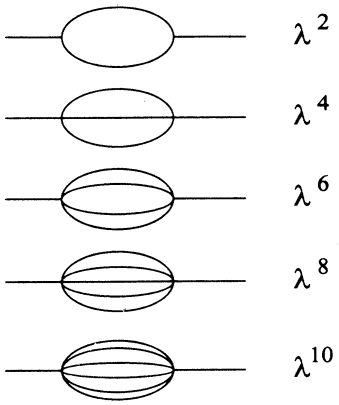

FIG. 1. Double-vertex diagrams.

The contribution $\Gamma_q^{(n)}$ to the damping Γ_q, due to the double-vertex diagram of vertex order n (with $n \geq 3$), is of perturbation order $\lambda^{2(n-2)}$. In the Appendix it is shown that the contribution $\Gamma_q^{(n)}$ to the damping is

$$\Gamma^{(n)}(\omega_q, \mathbf{k}_q) = \pi(n-1)!n^2 \sum_{2\cdots n} V_{q2\cdots n} V_{-q-2\cdots -n} \langle [b_2 \cdots b_n, b_{-2} \cdots b_{-n}] \rangle \times \delta[\omega_q - (\omega_2 + \cdots + \omega_n)] \delta[\mathbf{k}_q - (\mathbf{k}_2 + \cdots + \mathbf{k}_n)] \ . \tag{2.4}$$

The angular brackets denote a thermal average over the harmonic canonic ensemble and $V_{q2\cdots n}$ is the nth order anharmonic coupling coefficient. The δ function $\delta[\mathbf{k}_q-(\mathbf{k}_2+\cdots+\mathbf{k}_n)]$ indicates that the coefficients V vanish if the total momentum is not conserved. By summing on both positive and negative branch indices, Eq. (2.4) describes any combination of phonon creation and annihilation processes in which phonon q decays with conservation of energy and momentum. In other words, all combinations of phonons and antiphonons are considered.

Equation (2.4) has the form of a weighted multiphonon density of states, involving $n-1$ phonons. As shown in Ref. 20, such a density of states may be computed in a time which is linear, rather than exponential, in n if the weight function

$$V_{q2\cdots n}V_{-q-2\cdots-n}\langle[b_2\cdots b_n,b_{-2}\cdots b_{-n}]\rangle$$

is in the factorized form $\prod_l f(\omega_l,\mathbf{k}_l)$. In the following we will show that the thermal average $\langle[b_2\cdots b_n,b_{-2}\cdots b_{-n}]\rangle$ can be expressed in this form, while the coefficients V can be factorized under some approximation.

Expanding the commutator, the thermal average in Eq. (2.4) becomes

$$\langle[b_2\cdots b_n,b_{-2}\cdots b_{-n}]\rangle=\langle b_2\cdots b_nb_{-2}\cdots b_{-n}\rangle-\langle b_{-2}\cdots b_{-n}b_2\cdots b_n\rangle\ . \tag{2.5}$$

In the limit of large samples, Wick's theorem holds.[28,29] In this case, among all possible pairing schemes, the only non-negligible contribution to the thermal average in Eq. (2.5) is

$$\langle[b_2\cdots b_n,b_{-2}\cdots b_{-n}]\rangle=\langle b_2b_{-2}\rangle\cdots\langle b_nb_{-n}\rangle-\langle b_{-2}b_2\rangle\cdots\langle b_{-n}b_n\rangle\ . \tag{2.6}$$

The averages in Eq. (2.6) may be evaluated by going back to the traditional b, $b^\dagger$ notation:

$$\langle b_{-l}b_l\rangle=\begin{cases}\langle b_l^\dagger b_l\rangle=n(\omega_l)\ , & \text{for } l>0\\ \langle b_{-l}b_{-l}^\dagger\rangle=n(\omega_{-l})+1\ , & \text{for } l<0\ .\end{cases} \tag{2.7}$$

The two cases of Eq. (2.7) may be cast in a unique expression as

$$\langle b_{-l}b_l\rangle=n(|\omega_l|)+\frac{1-\sigma_l}{2}=\frac{\sigma_l}{2}(g_l-1)\ , \tag{2.8}$$

where $n(\omega)\equiv1/(e^{\omega/kT}-1)$ is the Bose occupation number and we have defined the *odd* function g_l of the phonon energy ω_l as

$$g_l\equiv\sigma_l[2n(|\omega_l|)+1]=\frac{e^{\omega_l/kT}+1}{e^{\omega_l/kT}-1}\ . \tag{2.9}$$

Using Eq. (2.8) the thermal average (2.6) becomes

$$\langle[b_2\cdots b_n,b_{-2}\cdots b_{-n}]\rangle=\prod_{l=2}^{n}\frac{\sigma_l}{2}(g_l+1)-\prod_{l=2}^{n}\frac{\sigma_l}{2}(g_l-1)\ . \tag{2.10}$$

Equation (2.10) is a generalization of the thermal factor $\prod_l(n_l+1)-\prod_l n_l$ obtained by Nitzan *et al.*[30] for multiphonon decay. Nitzan's factor can be obtained by restricting Eq. (2.10) to positive branch indices (all $\sigma_l=1$). In this case the contribution to the linewidths is restricted to "down conversion" processes, in which the excited phonon decays by transferring all its energy ω to other phonons of energy $\omega_2,\omega_3,\ldots$, such that $\omega=\omega_2+\omega_3+\ldots$. Down conversion processes are the only effective mechanism in the low-temperature limit. Equation (2.10) is the thermal factor for a general multiphonon process, where the excited state may also absorb energy from the phonon thermal bath, allowing any combination of phonons and antiphonons (i.e., including "up conversion" processes).

Both terms in the thermal factor (2.10) are now in factor form. The next step in the transformation of Eq. (2.4) is factorizing the anharmonic coupling coefficients $V_{q2\cdots n}$.

As discussed in many standard texts,[4,31] the coupling coefficients are given by

$$V_{q2\cdots n}=\frac{C_{q2\cdots n}}{n!(\sigma_q\omega_q\sigma_2\omega_2\cdots\sigma_n\omega_n)^{1/2}}\ . \tag{2.11}$$

The factors σ_l take care of the fact that the phonon energies $|\omega_l|=\sigma_l\omega_l$ must be positive in Eq. (2.11). The $C_{q2\cdots n}$ coefficients are the derivatives of the crystal potential with respect to the normal coordinates, so that they depend in a complicated way on the details of the interaction potential, and thus on ω_l and $\mathbf{k}_l$. On the other hand, if coefficients are assumed to be uncorrelated to the thermal factor $\langle[b_2\cdots b_n,b_{-2}\cdots b_{-n}]\rangle$, they can be replaced in Eq. (2.4) by their average value. Such an assumption implies, through Eqs. (2.9) and (2.10), that the coupling coefficient should not be correlated to the phonon energy. This appears to be reasonable, with one exception. As discussed in Refs. 15, 32, and 33, and shown in Sec. III, the coefficients $C_{q2\cdots n}$ tend linearly to zero as one of the phonon energies tends to zero (i.e., an acoustic branch is involved); otherwise they depend weakly on the energy of the optical phonons. Therefore, we need an approximation that reproduces this behavior. We have chosen to represent $C_{q2\cdots n}$ as

$$C_{q2\cdots n}=C_n(q)\prod_{l=2}^{n}\frac{\sigma_l\omega_l}{\langle\sigma_l\omega_l\rangle}\ . \tag{2.12}$$

Here, $\langle\sigma_l\omega_l\rangle$ is the average frequency for the branch i_l. This equation may be regarded as a definition of $C_n(q)$, whose value is obtained by averaging the square of (2.11) over phonons $2,\ldots,n$:

$$C_n(q)=\langle|C_{q2\cdots n}|^2\rangle^{1/2} \tag{2.13}$$

(each $\sigma_l\omega_l/\langle\sigma_l\omega_l\rangle$ factor obviously averages to 1).

Equation (2.12) is probably the simplest choice, which gives an approximately constant $C_{q2\cdots n}$ of the correct magnitude if no acoustic phonon is involved and has the correct behavior for low-frequency acoustic phonons. We tried more complicated forms, which when applied to nitrogen gave essentially identical results.

Using Eqs. (2.10) and (2.11) and approximation (2.12), expression (2.4) for the n-phonon damping becomes

$$\Gamma^{(n)}(\omega_q,\mathbf{k}_q)=\frac{\pi}{(n-1)!|\omega_q|}C_n^2(q) \times[G_+^{(n)}(\omega_q,\mathbf{k}_q)-G_-^{(n)}(\omega_q,\mathbf{k}_q)] , \quad (2.14)$$

where

$$G_\pm^{(n)}(\omega,\mathbf{k})=\sum_{2\cdots n}\delta[\omega-(\omega_2+\cdots+\omega_n)] \times\delta[\mathbf{k}-(\mathbf{k}_2+\cdots+\mathbf{k}_n)]\prod_{l=2}^{n}g_\pm(\omega_l) , \quad (2.15)$$

$$g_\pm(\omega_l)=(g_l\pm1)\frac{\omega_l}{2\langle\sigma_l\omega_l\rangle^2} . \quad (2.16)$$

The $G_\pm^{(n)}(\omega,\mathbf{k})$ functions are weighted densities of states with a factorized weight. As shown in Ref. 20, such densities may be efficiently computed one after the other using the recursive relation

$$G_\pm^{(n)}(\omega,\mathbf{k})=\sum_{\mathbf{k}_n i_n}G_\pm^{(n-1)}(\omega-\omega_{\mathbf{k}_n i_n},\mathbf{k}-\mathbf{k}_n)g_\pm(\omega_{\mathbf{k}_n i_n}) . \quad (2.17)$$

The recursive algorithm was originally conceived for positive energies. However, the sign of the energy is not really used in Ref. 20. Hence, Eq. (2.17) holds exactly in the same form for densities of *sum and difference* states, i.e., allowing both positive and negative energies. Using Eq. (2.17), each additional density $G_\pm^{(n)}$ can be computed recursively with a constant computational cost from the previous density $G_\pm^{(n-1)}$. The lowest-order density $G_\pm^{(2)}$ is computed directly from Eq. (2.15). The n-phonon damping is then obtained as a difference of $G_+^{(n)}$ and $G_-^{(n)}$ densities (Eq. 2.14). The recursive relation (2.17) yields the weighted densities for all $\mathbf{k}$ vectors, since these densities are required in each recursive step. As shown in the next section this gives the possibility of studying the dependence of $G_\pm^{(n)}(\omega,\mathbf{k})$ on n, ω, and $\mathbf{k}$.

III. CALCULATIONS: THE CASE OF NITROGEN

We have used Eq. (2.14) to compute the linewidths of the Raman-active modes in α-nitrogen up to vertex order $n=7$ (i.e., λ^{10}) and compared the result to the experimental data. Solid nitrogen in its α phase crystallizes as a cubic lattice (space group $Pa3$) and is stable in the temperature range 0–36 K (Ref. 35). Due to the presence of the center of inversion the phonons exhibit mutually exclusive Raman or ir activity. The one-phonon density of states has a very simple structure, the region of the lattice modes (0–70 cm^{-1}) being well separated from the sharp peak (2328–2329 cm^{-1}) due to the internal branches. With such an energy distribution, as we shall discuss in detail later, the double-vertex diagrams should give the main contribution to the linewidths of the vibron. Several potential models for nitrogen are available in the literature.[13,15,34–36] We have used the potential model of Murthy.[36] In this model the intermolecular interactions are represented by a Lennard-Jones atom-atom potential plus an electrostatic term represented by point charges along the molecular axis. We add a harmonic intramolecular potential, with a constant of 2328 cm^{-1}. The potential reproduces satisfactorily the structure of the solid at 5 K (Ref. 37) and the harmonic frequencies at zero wave vector and at the Brillouin-zone boundary.[35] All calculations have been performed at the extrapolated 0 K structure.[37]

As shown by Eq. (2.14), the damping $\Gamma_q^{(n)}$ is controlled by, (1) the magnitude of the average coupling coefficient $C_n(q)$, and (2) the thermally weighted density of states resonant with ω_q and $\mathbf{k}_q$, i.e., the factor

$$G^{(n)}(\omega,\mathbf{k})\equiv G_+^{(n)}(\omega,\mathbf{k})-G_-^{(n)}(\omega,\mathbf{k}) .$$

The calculation of $C_n(q)$ and $G^{(n)}(\omega,\mathbf{k})$ are two distinct and independent computational problems, which deserve to be discussed in some detail prior to presenting the results for the linewidths in α-nitrogen.

A. Average coupling coefficients

The relevant coefficients for $\mathbf{k}=0$ optical phonons are $C_n(q)$ with $q\equiv0i$. They can be obtained from a statistical sample of anharmonic coefficients $C_{q2\cdots n}$ [cf. Eq. (2.13)]. In principle, the nth order coefficients can be computed starting from the analytical form of the interaction potential;[4] however, the expressions for C become very complicated as n increases. We chose to calculate the coefficients in a simpler way by numerical derivation of second-order coefficients C_{12}.

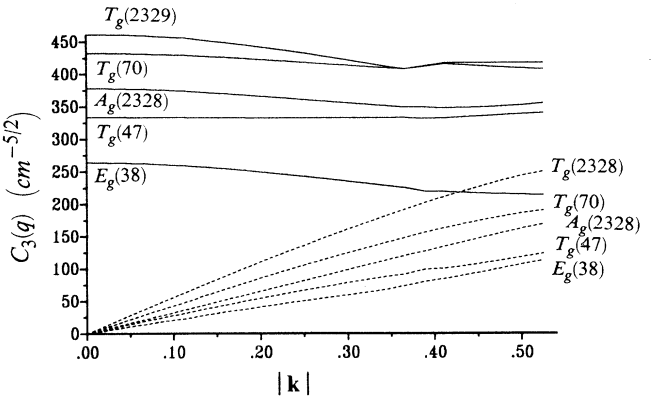

FIG. 2. Average third-order coupling coefficients $C_3(q)$ ($cm^{-5/2}$) for Raman modes as a function of the wave-vector modulus. Solid lines refer to coefficients $C_3(q,\mathbf{k})^2=N_{\text{opt}}^{-2}\sum_{i_1i_2}|C_3(0\mathbf{q},\mathbf{k}i_1,-\mathbf{k}i_2)|^2$ averaged over the optical branches i_1, i_2. Dashed lines refer to coefficients $C_3(q,\mathbf{k})^2=N_{\text{opt}}^{-1}\sum_{i_1}|C_3(0\mathbf{q},\mathbf{k}i_1,-\mathbf{k}i_2)|^2$ involving one acoustic branch i_2.

TABLE I. Average anharmonic coupling coefficients $C_n(q)^2$ for the Raman modes in α-nitrogen. The values in parentheses are the harmonic frequencies (cm^{-1}) predicted by Murthy's model (Ref. 36). The $C_n(q)^2$ coefficients are in units of $cm^{-(n+2)}$.

n	$T_g(2329)$	$A_g(2328)$	$T_g^+(70)$	$T_g^-(47)$	$E_g(38)$
3	1.53×10^5	9.98×10^4	6.68×10^4	5.36×10^4	4.51×10^4
4	6.76×10^5	2.33×10^5	8.09×10^5	4.83×10^5	2.27×10^5
5	2.45×10^6	1.53×10^6	4.41×10^6	1.48×10^6	2.68×10^5
6	9.66×10^6	7.01×10^5	3.39×10^7	1.08×10^7	6.01×10^5
7	3.64×10^7	6.14×10^5	1.54×10^8	6.42×10^7	6.34×10^6

Coefficients of the type $C_{12qq\cdots q}$, where $1\equiv\mathbf{k}i_l$, $2\equiv-\mathbf{k}i_2$, and $q\equiv0i$, can be easily obtained by computing the numerical derivatives of C_{12} with respect to the normal mode q. In practice, this amounts to computing the harmonic dynamical matrix C_{12} for different nonequilibrium positions of the atoms in the crystal, along the eigenvector q. The derivatives up to the order $2m$ can be obtained, with decreasing accuracy, from the value of C_{12} in $2m+1$ points $-mh,\ldots,-h,0,h,\ldots,mh$ along the collective coordinate q. As the displacement h approaches zero, the *a priori* error vanishes. On the contrary, the round-off error grows with h^{-1}.[38] So, in order to keep both errors small, a suitable compromise value of h must be chosen.

Only a particular class of coefficients can be computed with this procedure. Nevertheless, the statistics is not expected to be bad, as coefficients should depend only weakly on the selected sample. This appears to be the case, as it is shown in Fig. 2, which illustrates the wave-vector dependence of the third-order anharmonic coefficient in α-nitrogen. This figure also shows that the assumptions underlying Eq. (2.14), namely that the average coupling coefficients are linear in the energy of the acoustic phonons and weakly dependent on the energy of the optical phonons, are well satisfied already for $n=3$.

Using the procedure described above we computed the $C_n(q)$ coefficients in α-nitrogen with the potential of Murthy[36] by averaging over different values of i_1, i_2,$\mathbf{k}$ in $C_{12qq\cdots q}$. The coefficients up to vertex order $n=7$ are reported in Table I.

B. Many-phonon densities of states

The weighted multiphonon densities $G_\pm^{(n)}(\omega,\mathbf{k})$ have been computed using the recursive relation (2.17). The full Brillouin zone (BZ) of α-nitrogen was sampled with 1331 wave vectors (56 in the reduced BZ). Equation (2.17) allows one to obtain the density $G_\pm^{(n)}(\omega,\mathbf{k})$ for any phonon of energy ω and wave vector $\mathbf{k}$. As discussed in Ref. 20, the expensive part of the algorithm consists in the restricted summation over the wave vectors imposed by momentum conservation. This restriction, expressed by the Dirac's δ involving the wave vectors in Eq. (2.15), obliges one to perform two nested loops when using the recursive relation (2.17): the external index $\mathbf{k}$ runs over the reduced BZ, while the summation index $\mathbf{k}_n$ covers the full BZ. In Ref. 20, it was found for the unweighted densities of sum states that the $\mathbf{k}$-unrestricted density $G^{(n)}(\omega)=\langle G^{(n)}(\omega,\mathbf{k})\rangle$ becomes practically undistinguishable from $G^{(n)}(\omega,\mathbf{k})$ at high n. Since the weight factors $g_\pm(\omega_l)$ in Eq. (2.15) depend explicitly only on the phonon energy and not on the wave vector, we expected the $\mathbf{k}$-restricted weighted densities $G_\pm^{(n)}(\omega,\mathbf{k})$ to be similar to the $\mathbf{k}$-unrestricted weighted densities

$$G_\pm^{(n)}(\omega)\equiv\sum_{2\cdots n}\delta[\omega-(\omega_2+\cdots+\omega_n)]\prod_{l=2}^{n}g_\pm(\omega_l)$$
$$=\langle G_\pm^{(n)}(\omega,\mathbf{k})\rangle\ .$$

In order to verify this we have computed $G^{(n)}(\omega)$ by averaging the densities

$$G^{(n)}(\omega,\mathbf{k})=G_+^{(n)}(\omega,\mathbf{k})-G_-^{(n)}(\omega,\mathbf{k})$$

over all wave vectors in the reduced BZ at $T=36$ K, for several selected frequencies in the region of the lattice and internal modes (Table II). The standard deviations are always smaller than the corresponding average densities and decrease very rapidly with increasing n. Since the densities $G^{(n)}(\omega,\mathbf{k})$ are practically independent of the wave vector already at $n=4$, for high orders they may be safely computed by summing over the frequencies with no wave-vector restriction, through the recursive relation[20]

$$G_\pm^{(n)}(\omega)=\sum_{\mathbf{k}_n i_n}G_\pm^{(n-1)}(\omega-\omega_{\mathbf{k}_n i_n})\ .$$

TABLE II. $\mathbf{k}$-averaged weighted densities $G'^{(n)}(\omega)\equiv G_+^{(n)}(\omega)-G_-^{(n)}(\omega)$ at $T=36$ K and corresponding standard deviations (in parentheses), in units of cm^{n+1} for the Raman frequencies (cm^{-1}).

n	$\omega=38$	$\omega=47$	$\omega=70$	$\omega=2329$
3	2.28×10^{-5}	2.32×10^{-5}	9.73×10^{-5}	0.00
	(4.80×10^{-6})	(7.55×10^{-6})	(4.97×10^{-6})	(0.00)
4	1.93×10^{-5}	1.89×10^{-5}	1.06×10^{-5}	2.90×10^{-8}
	(6.51×10^{-8})	(1.83×10^{-7})	(1.22×10^{-7})	(2.32×10^{-10})
5	1.13×10^{-6}	1.14×10^{-6}	1.72×10^{-6}	1.24×10^{-9}
	(7.85×10^{-10})	(2.05×10^{-9})	(3.56×10^{-10})	(4.77×10^{-13})
6	1.65×10^{-7}	1.66×10^{-7}	1.37×10^{-7}	3.19×10^{-10}
	$(5.38e\times10^{-12})$	(4.66×10^{-11})	(2.72×10^{-11})	(8.24×10^{-14})
7	9.94×10^{-9}	1.01×10^{-8}	1.23×10^{-8}	1.87×10^{-11}
	(1.02×10^{-13})	(2.98×10^{-13})	(4.68×10^{-14})	(6.38×10^{-17})

Such a result might be important for future developments, since the recursive computation of weighted densities without wave vector constraints is much less time consuming and memory demanding.[20] We have not used this shortcut in this work, which employed the constrained sums of Eq. (2.17). The validity of the shortcut was by no means obvious *a priori.*

IV. RESULTS

We now discuss the temperature dependence of the linewidths due to the double-vertex diagrams up to the order $n=7$ (λ^{10}) obtained for the Raman modes in α-nitrogen and compare the results to the experimental data. The linewidths have been computed, using Eq. (2.14), for temperatures in the range 0–36 K, by multiplying the density $G^{(n)}(\omega,\mathbf{0})$ at the harmonic frequency ω_q by the average anharmonic coefficients $C_n(q)$, q referring to the Raman-active branches (Table I).

We also computed the unweighted multiphonon densities of states

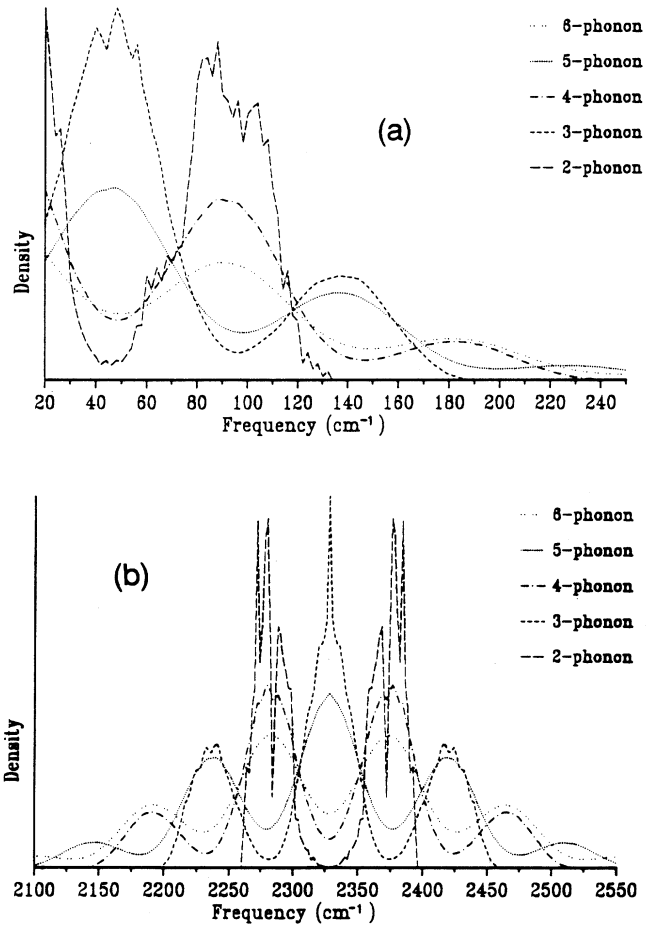

FIG. 3. n-phonon density of states $D^{(n)}(\omega,\mathbf{0})$, $n=2,\ldots,6$, in the region of the lattice modes (a) and of the vibrons (b). All densities are normalized to unit area.

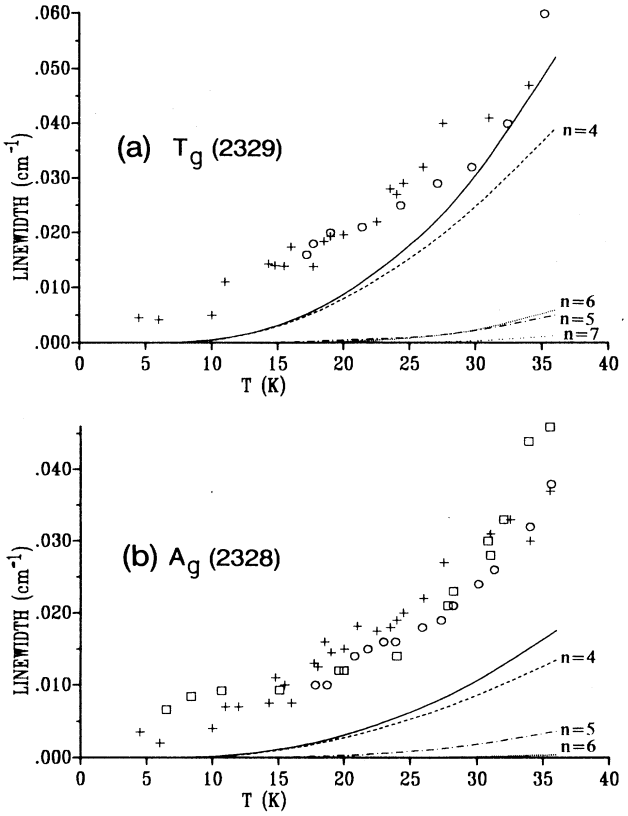

FIG. 4. Linewidth vs temperature for the Raman modes of α-nitrogen in the vibron region. Experimental: (Ref. 23) (crosses); (Ref. 24) (circles); (Ref. 25) (squares). Calculated: contributions due to single diagrams (broken lines); total linewidth (solid lines).

$$D^{(n)}(\omega,\mathbf{k})=\sum_{2\cdots n}\delta[\omega-(\omega_2+\cdots+\omega_n)]\times\delta[\mathbf{k}-(\mathbf{k}_2+\cdots+\mathbf{k}_n)]\,,$$

using, again, the recursive equation (2.17), with $g(\omega)=1$. These densities of states are not required for the computation of $\Gamma_q^{(n)}$ and have been calculated for the sole purpose of understanding the effects of the phonon dispersion. The densities are shown in Figs. 3(a) and 3(b) for the lattice and internal modes, respectively.

As expected, qualitatively and quantitatively different results were obtained for the linewidths of the vibron (Fig. 4) and of the lattice modes (Fig. 5). We shall discuss them separately.

A. Relaxation of the vibron

The linewidths up to the order λ^{10} for the vibrons T_g(2329 cm^{-1}) and A_g (2328 cm^{-1}) are shown in Fig. 4, together with the experimental data.[23–25] The temperature behavior of the T_g mode linewidth [Fig. 4(a)], obtained by summing the double-vertex diagrams, compares well to the experiments for $T\geq 20$ K. The discrepancies at low temperature are probably due to a residual

temperature-independent inhomogeneous contribution to the experimental linewidths.

For the A_g vibron, the agreement between data and calculations is not as good [Fig. 4(b)]. Due to the small dispersion of the internal modes [about 1 cm^{-1} (Refs. 39 and 40)], the A_g and T_g vibrons encounter the same resonances; any difference in the linewidths is therefore due to differences in the coupling coefficients. As shown in Table I, the average coupling coefficients involving the A_g mode are systematically smaller than those for the T_g mode and, correspondingly, larger linewidths are predicted for the latter. This prediction agrees qualitatively, but not quantitatively, with experiments:[23–25] the experimental linewidths of the A_g mode are smaller than that of the T_g mode, but still larger than their theoretical counterparts [Fig. 4(b)].

Analyzing the contributions $\Gamma^{(n)}$ to the width of the vibrons T_g and A_g, we find that in both cases the dominant contribution is given by the diagram of vertex order $n=4(\lambda^4)$, the $n=3,5,6,7$ terms being much smaller (Fig. 4). Due to the absence of three-phonon resonances around 2328–2329 cm^{-1} [Fig. 3(b)], $\Gamma^{(3)}$ is practically zero at any temperature. It should be noticed that the multiphonon densities [Fig. 3(b)] involving $n-1$ phonons with n odd have a deep minimum at the energy of the vibrons. Accordingly, the damping terms with odd vertex order are expected to be small.

The agreement between calculations and experiments leads us to believe that in general the line broadening of isolated vibrons is due to double-vertex diagrams with even vertex order. We attribute this phenomenon to the behavior of the multiphonon density of states at the energy of the decaying vibron, which severely restricts the number of effective diagrams. At the λ^4 level, for example, all diagrams describing decay processes,[9,11,21] except the double-vertex diagram with $n=4$, have at least one third-order external vertex (involving a two-phonon density of states) and therefore do not contribute to the vibron linewidth.

B. Relaxation of the Raman lattice modes

The various contributions to the damping for the three Raman-active lattice modes as a function of temperature are shown in Figs. 5(a)– 5(c). The good agreement between experimental and computed linewidths for the lattice modes was a surprise. In the case of lattice phonons, where three-phonon processes are allowed, it is generally believed[11,10] that the main contribution to the linewidth beyond λ^2 order is given by diagrams involving cubic vertices, which were not included in the present treatment. Therefore, we were expecting a substantial discrepancy between computed and experimental linewidths for all the lattice phonons.

Obviously, the observed agreement may be due to cancellation of errors, e.g., an excess of anharmonicity in the $C_n(q)$ coefficients may compensate the missing contribution arising from the diagrams not included in the present calculation. On the other hand, a possible explanation of the good agreement in the case of the E_g mode at 38 cm^{-1} (computed frequency), for which experimental data are available up to the transition temperature,[23,26] may be found in the behavior of the multiphonon density of states. In the region of the lattice modes [see Fig. 3(a)], the density around 38 cm^{-1} shows a behavior similar to that observed at the energy of the vibron, with alternating minima (for n-phonon densities with even n) and maxima (odd n). Thus, we might infer that, similarly to the case of the vibron just discussed, more complex diagrams containing an odd external vertex give negligible

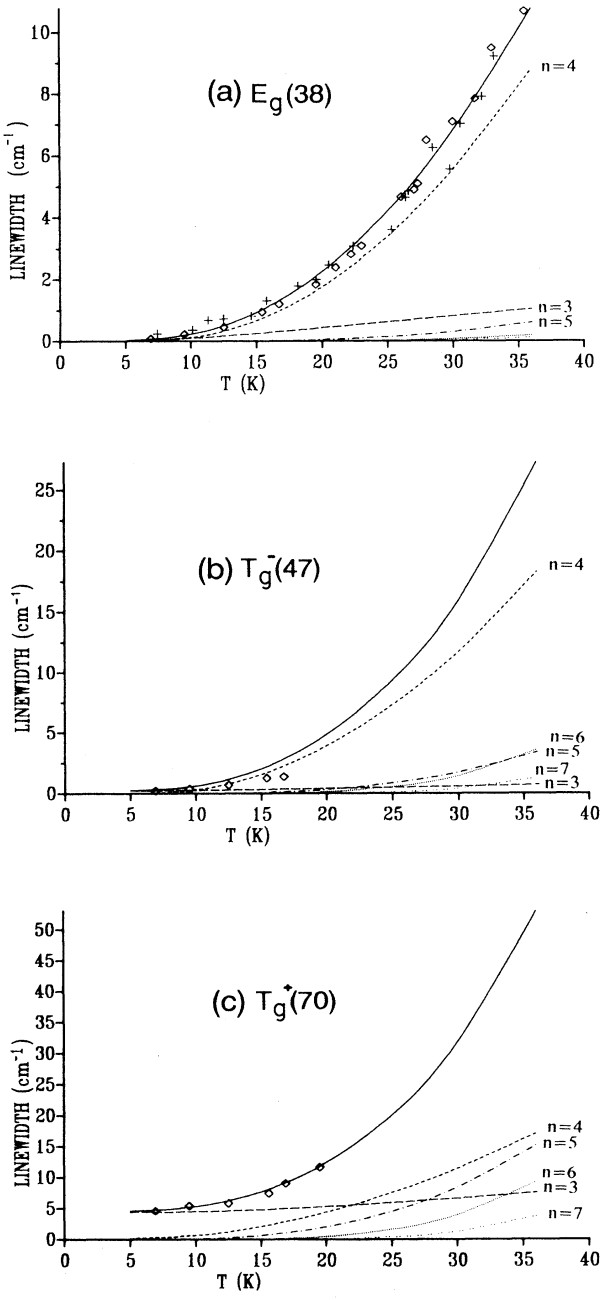

FIG. 5. Linewidth vs temperature for the Raman modes of α-nitrogen in the lattice region. Experimental: (Ref. 23) (crosses); (Refs. 26 and 27) (diamonds). Calculated: contributions due to single diagrams (broken lines); total linewidth (solid lines).

contribution, and the relaxation is mostly due to the double-vertex diagram of order $n=4$.

Also in the case of the T_g^- phonon at 47 cm^{-1}, the major contribution to the linewidths is given by the $n=4$ term [Fig. 5(b)]; again, the phonon energy occurs approximately in correspondence of minima or maxima of the multiphonon densities of the states. Unfortunately, the experimental linewidths[27] are available only up to 17 K, so the comparison with the computation is problematic.

For the T_g^+ mode at 70 cm^{-1}, the predicted linewidth at low temperature agrees well with experiment [Fig. 5(c)].[27] The contributions of order higher than λ^4 are in this case quite large. The residual linewidth at 0 K is entirely due to two-phonon decay processes ($n=3$); such processes are very likely to occur, as it can be seen from the sizeable two-phonon density [Fig. 3(a)] around 70 cm^{-1}. As for the T_g^- phonon, also in the case of the T_g^+ mode, the temperature range of the experimental data (0–20 K) is too narrow to allow definitive conclusions about the relaxation processes involved to be drawn.

V. CONCLUSIONS

The main result of this work is the theoretical and practical demonstration of the fact that very high-order corrections to the phonon self-energy may be efficiently computed even for a system as complex as a molecular crystal. Due to the presence of nested sums on intermediate states, the computation of corrections of order λ^n with traditional algorithms requires a time which grows exponentially with n. We have found that this nested-sum difficulty may be overcome for the special case of the double-vertex diagrams. In this case a recursive algorithm may be used, which allows the linewidths up to order λ^n to be computed in time *linear,* rather than *exponential,* in n.

We have computed the linewidths up to the order λ^{10} due to the double-vertex diagrams for α-nitrogen. The computed linewidths and their temperature dependence are in good agreement with the experiment. We have used a potential model[36] adjusted to the structure and *harmonic* frequencies of α-N_2. No adjustable parameter is involved in our calculations, which may therefore be regarded as an *a priori* determination of the linewidths. Previous calculations for nitrogen showed that different potential models with comparable harmonic frequencies may give significantly different linewidths at the λ^2 level.[13,15] Consequently, we believe the very good results obtained using Murthy's potential[36] to be partially fortuitous. Nevertheless, we think that the overall behavior of the linewidths is independent on the details of the potential model and that some observations of general validity may be drawn.

(1) The damping term of order n tends to zero with increasing n. However, the convergence of the series is not necessarily fast. For nitrogen the adimensional convergence ratios $\lambda=C_{n+1}(q)/\omega C_n(q)$ between consecutive average coefficients are in the range 0.03–0.3, ω being the energy of a typical lattice mode, say $\omega=50$ cm^{-1}. Thus the convergence of the double-vertex series is generally rather slow, especially at high temperature ($kT \gtrsim \omega$).

(2) The convergence of the double-vertex series is reached much faster, generally at the λ^4 level, for "isolated" phonons. These phonons are isolated in the sense that they escape decay processes involving vertices of odd order, due to the shape of the n-phonon densities of states. This is often the case for vibrons.

ACKNOWLEDGMENTS

This work was supported by Italian CNR and MURST. We thank Jan De Kinder and Etienne Goovaerts for providing data prior to publication and for invaluable help in improving the quality and scope of this work. We are also indebted to Vincenzo Schettino for helpful discussion and precious suggestions.

APPENDIX: DOUBLE-VERTEX SELF-ENERGY

Frequent references in the form (I. . .) to equations in the previous paper[21] (Ref. I) will occur in this appendix. The basic equation of this work [Eq. (2.4)] will be obtained by replacing twice Eq. (I4.8) into Eq. (I4.6), discarding all terms which do not represent double-vertex diagrams and rearranging the result. Thus, we start from the equation of motion [Eq. (I4.6)] for the one-phonon Green's function $G(q)=G(b_q,b_{-q};\omega)$:

$$(\omega-\omega_q)G(q)=1+\sum_{n\geq 3} n \sum_{23\cdots n} V_{-q23\cdots n}G(23\cdots n)\ . \tag{A1}$$

Then, using Eq. (I4.8) to climb one step in the hierarchy of coupled equations, we keep only those terms which may give rise to double-vertex diagrams when replaced in Eq. (A1):

$$G(23\cdots n)=\frac{1}{\omega-(\omega_2+\omega_3+\cdots+\omega_n)} n \sum_{2'\cdots n'} \{\sigma_2 V_{-22'\cdots n'}G(2'\cdots n'34\cdots n) + \sigma_3 V_{-32'\cdots n'}G(22'\cdots n'45\cdots n)+\cdots\}\ . \tag{A2}$$

For each one of the $n-1$ Green's functions on the right-hand side of Eq. (A2), we climb another step [Eq. (I4.8)] and discard all terms that give rise to diagrams with three or more vertices. For example, for the Green's function $G(22'\cdots n'45\cdots n)$ one obtains

$$G(22'\cdots n'45\cdots n)=\frac{1}{\omega-(\omega_2+\omega_{2'}+\cdots+\omega_{n'}+\omega_4+\omega_5+\cdots+\omega_n)}\langle[b_2 b_{2'}\cdots b_{n'} b_4 b_5\cdots b_n, b_{-q}]\rangle\ . \tag{A3}$$

In the limit of a large sample, Wick's theorem holds.[28,29] Then the only averages which are not negligible, and, which

give rise to double-vertex diagrams when replaced in Eqs. (A1) and (A2), are those where one of the $n-1$ summation indices $2'\cdots n'$ is conjugate to $-q$, while the other indices are conjugate to $245\cdots n$ [again for $G(22'\cdots n'45\cdots n)$]. Overall these conjugate pairings may take place in $(n-1)!$ different ways. In Eq. (A3) all the conjugate frequency pairs $\omega_j+\omega_{-j}$ vanish from the frequency factor, which becomes[21]

$$\frac{1}{\omega-(\omega_2+\omega_q+\omega_{-2}+\omega_{-4}+\cdots+\omega_{-n}+\omega_4+\cdots+\omega_n)}=\frac{1}{\omega-\omega_q}=G_0(q), \tag{A4}$$

where we have recognized $1/(\omega-\omega_q)$ as the "bare" Green's function $G_0(q)$. As discussed in Ref. 21, the decoupling procedure for the hierarchy of coupled equations for the Green's functions involves the replacement of $G_0(q)$ with the "dressed" function $G(q)$. After this replacements, repeating the above procedure for all terms in Eq. (A2), exploiting the symmetry of $V_{12\cdots n}$ with respect to exchanges of indices, and taking into account the multiplicity factor $(n-1)!$, we obtain the equation for $G(q)$:

$$\begin{aligned}(\omega-\omega_q)G(q)=1+\sum_{n\geq 3} n^2(n-1)!\sum_{23\cdots n} V_{-q23\cdots n}V_{q-2-3\cdots-n}\frac{1}{\omega-(\omega_2+\omega_3+\cdots+\omega_n)}\\ \times\{\sigma_2\langle[b_q b_{-3}b_{-4}\cdots b_{-n}b_3b_4\cdots b_n,b_{-q}]\rangle\\ +\sigma_3\langle[b_2b_qb_{-2}b_{-4}b_{-5}\cdots b_{-n}b_4b_5\cdots b_n,b_{-q}]\rangle+\cdots\}G(q)\,.\end{aligned} \tag{A5}$$

By comparing Eq. (A5) with the expected Dyson's equation $(\omega-\omega_q)G(q)=1+\Sigma(q)G(q)$, we identify the coefficient of $G(q)$ as the self-energy due to the double-vertex diagrams $\Sigma(q)$.

The averages in Eq. (A5) may be simplified using Wick's theorem, which allows us to commute inside the thermal averages all pairs of b_l operators, except those with conjugate summation indices. For conjugate indices, according to Eq. (I2.8), $[b_l,b_{-l}]=\sigma_l$. Furthermore $\sigma_q=1$, as $q>0$. Thus the expression in braces in Eq. (A5) becomes

$$\{\cdots\}=\sigma_2\langle b_{-3}b_{-4}\cdots b_{-n}b_3b_4\cdots b_n\rangle+\sigma_3\langle b_2b_{-2}b_{-4}\cdots b_{-n}b_4\cdots b_n\rangle+\cdots\,. \tag{A6}$$

Equation (A6) may be transformed in a more compact form by noticing that, thanks to Eq. (IA1),

$$[b_2b_3\cdots b_n,b_{-2}b_{-3}\cdots b_{-n}]=[b_2,b_{-2}b_{-3}\cdots b_{-n}]b_3\cdots b_n+b_2[b_3,b_{-2}b_{-3}\cdots b_{-n}]b_4\cdots b_n+\cdots\,. \tag{A7}$$

It is easy to see, using again Eq. (I2.8) and Wick's theorem, that the average of the summation on right-hand side of Eq. (A7) is equal to $\{\cdots\}$ [Eq. (A6)]. Thus we may rewrite the self-energy $\Sigma(q)$ as

$$\Sigma(q)=\sum_{n\geq 3} n^2(n-1)!\sum_{23\cdots n} V_{-q23\cdots n}V_{q-2-3\cdots-n}\langle[b_2b_3\cdots b_n,b_{-2}b_{-3}\cdots b_{-n}]\rangle\frac{1}{\omega-(\omega_2+\omega_3+\cdots+\omega_n)}\,. \tag{A8}$$

Our main equation for the nth-order damping term $\Gamma_q^{(n)}$ [Eq. (2.4)] is obtained directly as the imaginary part[3] of the nth term of the series for $\Sigma(q)$ [Eq. (A8)].

[1]S. Califano and V. Schettino, Int. Rev. Chem. **7-1**, 19 (1988).
[2]P. Foggi and V. Schettino, Riv. Nuovo Cimento **15**, No. 7 (1992).
[3]A. A. Maradudin and A. Fein, Phys. Rev. **128**, 2589 (1962).
[4]S. Califano, V. Schettino, and N. Neto, *Lattice Dynamics of Molecular Crystals* (Springer-Verlag, Berlin, 1981).
[5]D. N. Zubarev, Usp. Fiz. Nauk **71**, 71 (19) [Sov. Phys. Usp. **3/3**, 320 (1960)].
[6]S. V. Tyablikov and V. L. Bonch-Bruevich, Adv. Phys. **11**, 317 (1962).
[7]S. W. Lovesey, *Condensed Matter Physics* (Benjamin, Reading, MA, 1980).
[8]L. Van Hove, Phys. Rev. **95**, 249 (1954).
[9]R. S. Tripathy and K. N. Pathak, Nuovo Cimento **21**, 286 (1974).
[10]V. K. Jindal, R. Righini, and S. Califano, Phys. Rev. B **38**, 4529 (1989).
[11]M. Monga and K. N. Pathak, Phys. Rev. B **18**, 5859 (1978).
[12]P. Procacci, G. Cardini, R. Righini, and S. Califano, Phys. Rev. B **45**, 2113 (1992).
[13]K. Kobashi, Mol. Phys. **36**, 225 (1978).
[14]K. Kobashi and V. Chandrasekharan, Mol. Phys. **36**, 1645 (1978).
[15]G. F. Signorini, P. F. Fracassi R. Righini, and R. G. Della Valle, Chem. Phys. **100**, 315 (1985).
[16]R. G. Della Valle, P. F. Fracassi, R. Righini, and S. Califano, Chem. Phys. **74**, 179 (1983).
[17]R. Righini, Chem. Phys. **84**, 97 (1984).
[18]P. Procacci, R. Righini, and S. Califano, Chem. Phys. **116**, 171 (1987).
[19]G. F. Signorini, R. Righini, and V. Schettino, Chem. Phys. **154**, 245 (1991).
[20]R. G. Della Valle and G. Cardini, Phys. Rev. Lett. **59**, 2196 (1987).
[21]R. G. Della Valle and P. Procacci, Phys. Rev. B **46**, 6141 (1992).
[22]P. Procacci, A. Tafi, L. Angeloni, R. Righini, and P. R. Salvi, Chem. Phys. **154**, 331 (1991).
[23]R. Ouillon, C. Turc, J.-P. Lemaistre, and P. Ranson, J. Chem. Phys. **93**, 3005 (1990).
[24]R. D. Beck, M. F. Hineman, and J. W. Nibler, J. Chem. Phys. **92**, 7068 (1990).
[25]J. De Kinder, E. Goovaerts, A. Bouwen, and D. Schoemaker, Phys. Rev. B **42**, 5953 (1990).

[26]J. De Kinder, E. Goovaerts, A. Bouwen, and D. Schoemaker, J. Lumin. **53**, 72 (1992).
[27]J. De Kinder and E. Goovaerts (private communication).
[28]W. E. Parry, *The Many-Body Problem* (Oxford Science, Oxford, 1973).
[29]A. A. Abrikosov, L. P. Gorkov, and I. E. Dzyaloshinski, *Methods of Quantum Field Theory in Statistical Mechanics* (Prentice-Hall, Englewood Cliffs, NJ, 1963).
[30]A. Nitzan, S. Mukamel, and J. Jortner, J. Chem. Phys. **60**, 3929 (1973).
[31]M. Born and K. Huang, *Dynamical Theory of Crystal Lattices* (Oxford University Press, New York, 1954).
[32]R. E. Peierls, *Quantum Theory of Solids* (Oxford University Press, New York, 1955).
[33]I. I. Ipatova, A. A. Maradudin, and R. F. Wallis, Fiz. Tverd. Tela (Leningrad) **8**, 1064 (19) [Sov. Phys. Solid State **8**, 850 (1965)].
[34]A. Ron and O. Schnepp, J. Chem. Phys. **42**, 3991 (1967).
[35]K. Kjems and G. Dolling, Phys. Rev. B **11**, 1639 (1975).
[36]C. S. Murthy, S. F. O'Shea, and I. R. McDonald, Mol. Phys. **50**, 531 (1983).
[37]I. N. Krupskii, A. I. Prokhvatilov, and A. I. Erenburg, Fiz. Nizk. Temp. **1**, 359 (1975) [Sov. J. Low Temp. Phys. **1**, 178 (1975)].
[38]A. Ralston and P. Rabinowitz, *A First Course in Numerical Analysis,* 2nd ed. (McGraw-Hill, New York, 1978).
[39]G. Zumofen, K. Dressler, M. M. Thiery, and V. Chandrasekharan, J. Chem. Phys. **67**, 6983 (1977).
[40]I. I. Abram, R. M. Hochstrasser, J. E. Kohl, M. G. Semack, and D. White, J. Chem. Phys. **71**, 153 (1979).